JOURNAL OF MATERIALS SCIENCE 33 (1998) 3935–3943

Stress states in $RENi_5$ powders during hydrogen charging and discharging cycles

S. B. BINER
Ames Laboratory, Iowa State University, Ames, IA 50011 USA
E-mail: biner@ameslab.gov

In this study, the evolution of the stress states in $RENi_5$ particles during hydrogen charging and discharging cycles were investigated using coupled diffusion–deformation finite-element method analyses. The results indicate that large tensile stresses, of the order of 20–30% of the modulus of elasticity, develop in the particles even in the absence of both internal and external crack-like defects. The internal and external cracks behave differently from each other during hydrogen charging and discharging cycles. Therefore, the fracture resistance of the particles containing external cracks will be different from the particles having internal cracks. The disc-shaped particles, in addition to having faster charging–discharging cycles, may offer better resistance to fracture than the spherical particles.

1. Introduction

The application of hydride-forming $RENi_5$ compounds, where RE denotes the rare earths La, Ce and misch-metals, in rechargeable nickel metal hydride batteries is well known [1–4]. In the case of $LaNi_5$, a large amount of hydrogen can be absorbed to form $LaNi_5H_{6.7}$ at nearly room temperature [1]. The calculated density of the absorbed hydrogen is a factor of about two higher than the density of liquid hydrogen [5]. The lattice dimensions of unsaturated $LaNi_5$ are $a \approx 5.017$ Å and $c \approx 3.982$ Å and, after saturation with hydrogen, the lattice parameters increase to $a \approx 5.440$ Å and $c \approx 4.310$ Å which represents a volume expansion of over 25% [3]. Associated with this large volume expansion, the hydrogenation cycles produce very fine powders through a cleavage fracture of initial particles, leading to reductions in battery performance.

In this study, to elucidate the stress states in the particles during the hydrogen charging and discharging cycles a set of coupled diffusion–deformation finite-element analyses are performed. The roles of crack location and the shape of the initial powders on the evolution of the stress states are also investigated.

2. Details of the finite-element method analyses

The hydrogen diffusion into $RENi_5$ is assumed to be a bulk diffusion process driven by chemical potential [5] which can be described by the general behaviour

$$J = -sD\left(\kappa_S \frac{\partial}{\partial x}(\ln \tilde{\theta}) + \frac{\partial \phi}{\partial x}\right) \tag{1}$$

where J is the flux concentration of the diffusing phase, $D(c, \tilde{\theta})$ is the diffusivity, $s(\tilde{\theta})$ is the solubility, $\kappa_S(c, \tilde{\theta})$ is the "Soret effect" factor providing diffusion because of a possible temperature gradient, $\tilde{\theta}$ is the absolute temperature and ϕ is the normalized concentration (often also referred to as the "activity" of the diffusing material), given by $\phi = c/s$ in which c is the mass concentration of the diffusing material in the base material. By changing variables (i.e., $c = \phi s$) and introducing the constitutive assumption as

$$\int_V \left[\delta\phi\left(s\frac{d\phi}{dt} + \phi\frac{ds}{d\tilde{\theta}}\frac{d\tilde{\theta}}{dt}\right) + \frac{\partial(\delta\phi)}{\partial x} sD \times \left(\frac{\kappa_S}{\tilde{\theta}}\frac{\partial\tilde{\theta}}{\partial x} + \frac{\partial\phi}{\partial x}\right)\right] dV = \int_s \delta\phi q \, dS \tag{2}$$

where

$$q = -nJ \tag{3}$$

which is the concentration flux entering the body across S and n is the unit normal vector.

In a finite-element analysis, equilibrium is approximated with a finite set of equations by introducing interpolation functions, N^N, and for the time integration, applying the Euler method, equation 2 can be rewritten as

$$\int_V \left[N^N\left(s\frac{(\phi_{t+\Delta t} - \phi_t)}{\Delta t} + \phi\frac{ds}{d\tilde{\theta}}\frac{d\tilde{\theta}}{dt}\right) + \frac{\partial N^N}{\partial x} sD \times \left(\frac{\kappa_S}{\tilde{\theta}}\frac{\partial\tilde{\theta}}{\partial x} + \frac{\partial\phi}{\partial x}\right)\right] dV = \int_s N^N q ds \tag{4}$$

where Δt is the time increment.

During the hydrogen charging and discharging cycles, the stress–strain behaviour of the powders is assumed to be elastic:

$$\sigma = \mathbf{D}[\varepsilon_D + \varepsilon_V(\phi)] \tag{5}$$

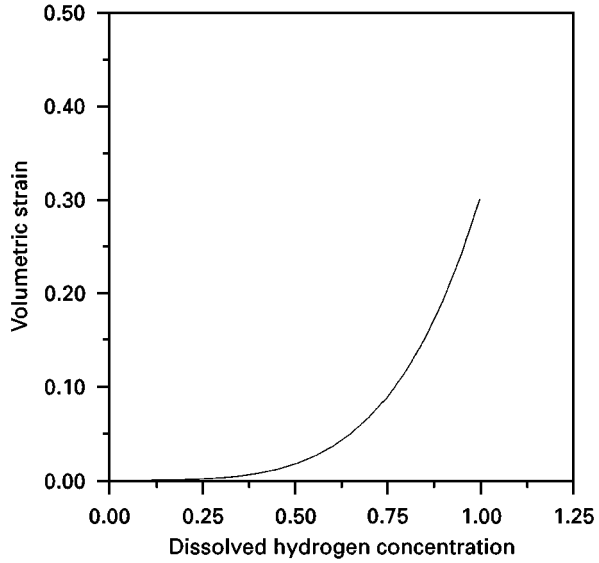

Figure 1 Assumed variation of the volumetric strain with hydrogen concentration.

where **D** is the elasticity matrix, ε_D is the deviatoric component of the total strain and $E_V(\phi)$ is the volumetric strain which is a function of the normalized hydrogen concentration. The relationship between the normalized hydrogen concentration and the volumetric strain in equation 5 is assumed to follow that given in Fig. 1. At low hydrogen concentrations the contribution of the diffusing hydrogen to volumetric expansion is small; however, this contribution increases exponentially, yielding about 25–30% volume expansion at the limit of solubility. Equations 4 and 5 coupled diffusion and deformation can be rewritten in the matrix form as

$$\begin{bmatrix} \mathbf{K}_D \\ \mathbf{K}_E \end{bmatrix} \begin{Bmatrix} \phi \\ u \end{Bmatrix} = \begin{Bmatrix} J \\ F \end{Bmatrix} \tag{6}$$

where $\mathbf{K}_D$ is the diffusion matrix and $\mathbf{K}_E$ is the elastic stiffness matrix, u is the displacement vector and F is the external applied load vector. During the analyses, it was assumed that both the diffusion parameters and the elastic properties remain constant in spite of possible phase changes; also, temperature effects were neglected. Throughout the study, the time values were normalized with the coefficient of the diffusion, all the stress values were normalized with the value of Young's modulus and the concentration values were normalized with the solubility value, thus yielding results that are independent of the material parameters.

3. Results

First, the evolution of the stress state in the spherical powders in the absence of any initial crack is studied. Because of the symmetry, only one quarter of the particle was modelled; the finite-element method (FEM) mesh used in the analyses, shown in Fig. 2, was composed of eight-node isoparametric elements. At the beginning of the solution, the hydrogen concentration inside the particle was assumed to be zero and the presence of an abundant supply of hydrogen at the particle boundary was provided. The distribution of the hydrogen concentration inside the spherical particle at various stages of the charging cycle is shown in Fig. 3. Owing to perfect spherical particle geometry, a uniform increase in the hydrogen concentration from the surface towards the centre with increasing time can be seen from the figure. Also, the volume expansion associated with the increase in the hydrogen concentration can be discerned from the figure. A 25% volume expansion corresponds to about 7.7% increase in the radius of the particle; the occurrence of this expansion for the almost fully charged stage, at a normalized time value of 0.295, can be seen in Fig. 3. The evolution of the normal stress during the charging cycle is shown in Fig. 4. The initial increase in the stress values occurs in regions near the surface because of the initial higher hydrogen concentration (Fig. 3) and, as the hydrogen concentration becomes more uniform, so does the stress distribution. Also, the formation of very high tensile stress values throughout the particle, about 20% of the modulus value, at an almost fully charged state can be seen from the figure.

In the next set of simulations the charging and discharging behaviour of the same spherical particles but containing a circumferential external crack and

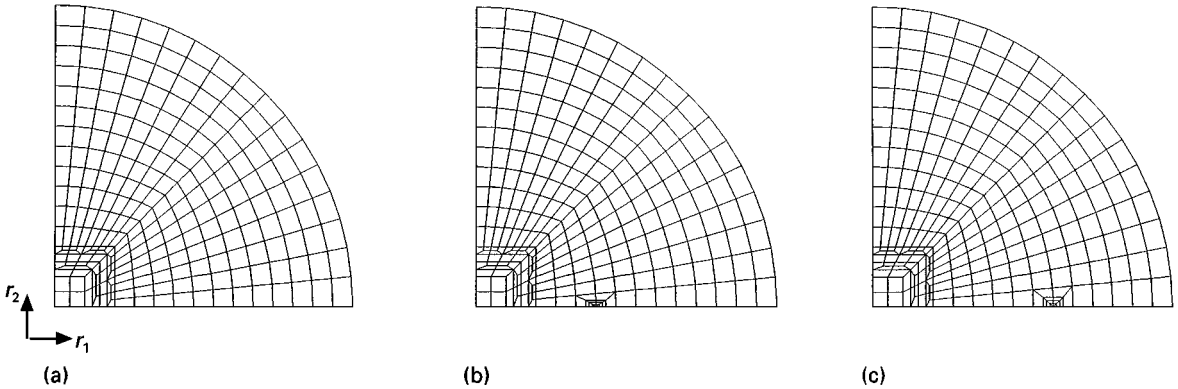

Figure 2 FEM meshes used in the analyses of the spherical particles: (a) particle without any crack; (b) particle with a penny-shaped internal crack; (c) particle with a circumferential external crack.

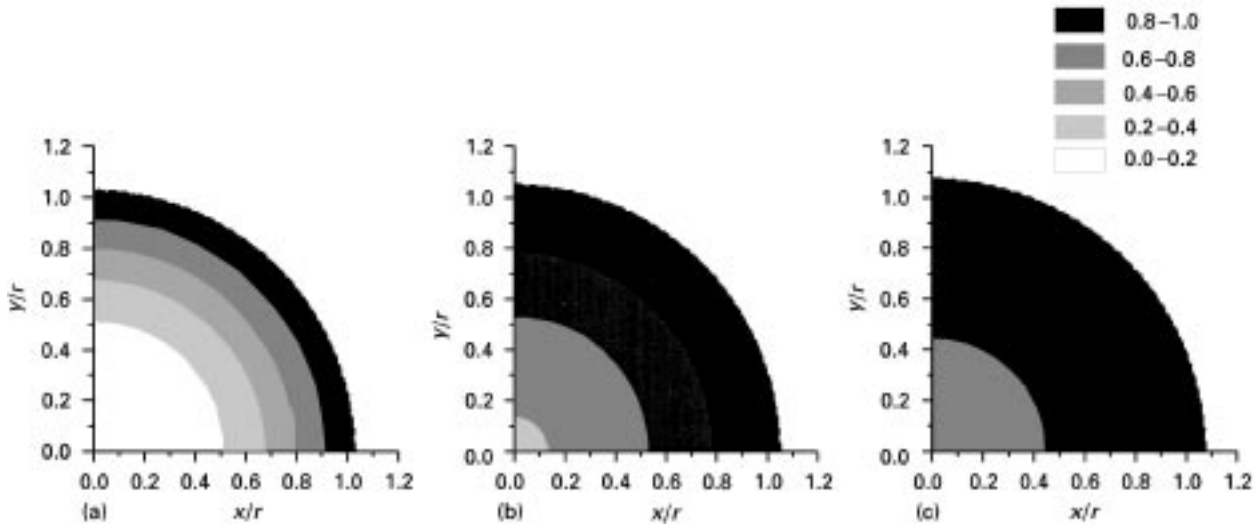

Figure 3 Variation in the hydrogen concentration throughout the spherical particle during the hydrogen-charging cycle for various normalized charging times: (a) 0.0484; (b) 0.0984; (c) 0.295.

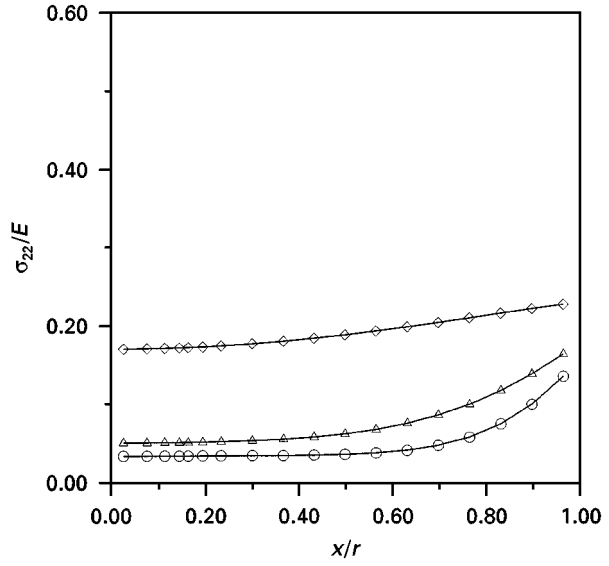

Figure 4 The variation in the normal stress throughout the spherical particle during the hydrogen-charging cycle for various normalized charging times. (○), 0.0484; (△), 0.0984; (◇), 0.295.

a penny-shaped internal crack were studied. For both cases, the crack lengths were the same; the FEM meshes used in these analyses are also shown in Fig. 2. To model the crack tip singularity, collapsed elements having shifted midside nodes [6] were used in the immediate crack tip region in these analyses. The penetration of the crack faces resulting from the volume expansion was prevented by using a series of non-dimensional interface elements [7] along the crack surfaces. Again, no hydrogen was present in the particles at the beginning of the solution, and the other boundary conditions were also the same as before. The distribution of the hydrogen concentration within the particle containing a circumferential external crack at various times during the charging cycle is shown in Fig. 5. The development of an initial non-uniform hydrogen distribution, in contrast with Fig. 3, owing to the diffusion of the hydrogen from the crack faces can be immediately recognized from the figure. Again, for this cracked particle, about an 8% increase in the particle radius was observed in a nearly fully charged state. Fig. 6 shows the variation in the normal stresses in the crack plane along the radial distance during the same hydrogen-charging cycle. In the figure, the crack tip is located at $x/r = 0.6$, where r is the radius of the particle; x/r values greater than this value represent the crack wake region and smaller values are for the regions ahead of the crack tip. As can be seen from the figure, as a result of hydrogen diffusion from the crack faces, the maximum stress value in the crack wake region was attained in a very short time period. On the other hand, the magnitude of the tensile normal stress ahead of the crack tip region was not different from that seen in Fig. 4 for a spherical particle without any crack in the fully charged state. This behaviour is the result of the crack-opening behaviour during the charging cycle as shown in Fig. 7. As can be seen from Fig. 7, at extremely early stages of the charging cycle the crack faces partially open. Later, because of swelling of the crack faces resulting from the volume expansion, the crack faces close again and remain closed throughout the remaining portion of the charging cycle.

Fig. 8 shows the variation in the hydrogen concentration in the crack plane during the discharging of the same particle. This was achieved by reducing the available hydrogen concentration to zero at the free surfaces during the analyses. In the figure, the zero value of the normalized time corresponds to the fully charged state. The variation in the normal stresses in the crack plane for the same time periods seen in Fig. 8 is shown in Fig. 9. As can be seen from the figure, the stress values in the wake region were reduced to zero almost immediately. On the other hand, there was an increase in the stress values at regions very near the crack tip. This increase approached a value of almost half the modulus of elasticity. This elevation again occurred almost at the beginning of the discharging cycle; with further loss of hydrogen, an

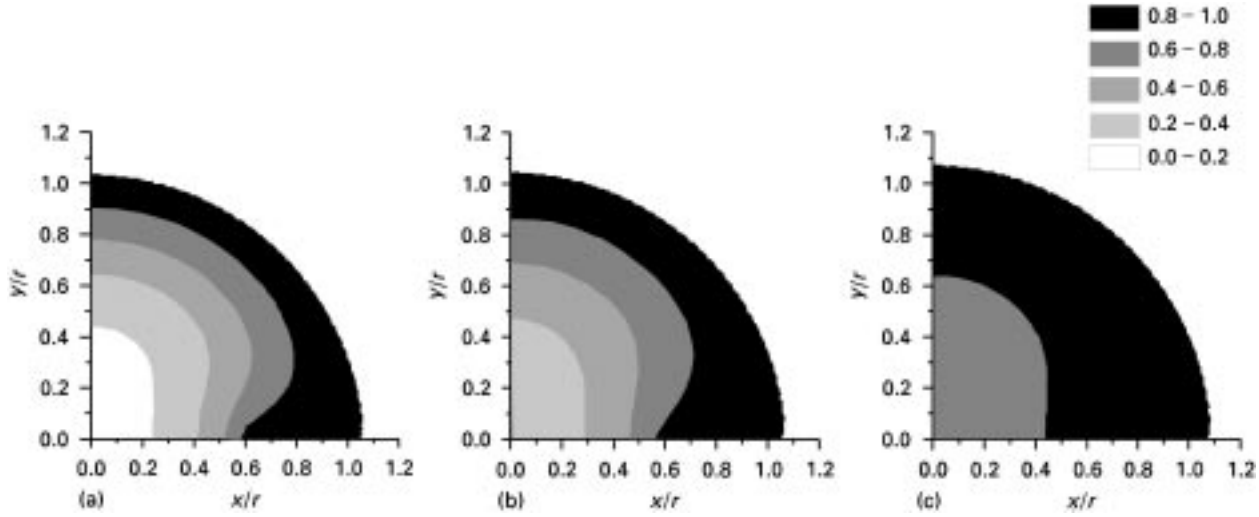

Figure 5 Variation in the hydrogen concentration throughout the spherical particle containing a circumferential external crack during the hydrogen-charging cycle for various normalized charging times: (a) 0.0234; (b) 0.0734; (c) 0.2220.

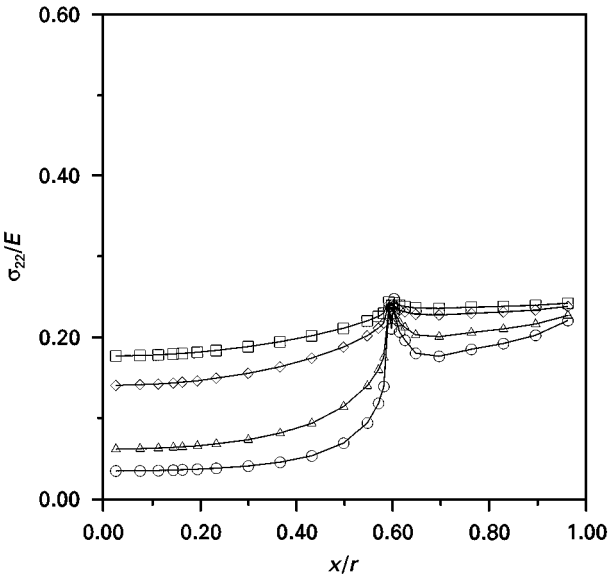

Figure 6 Evolution of the stress state in the spherical particle with circumferential external crack during the hydrogen-charging cycle for various normalized charging times. (○), 0.0234; (△), 0.0734; (◇), 0.1720; (□), 0.2220.

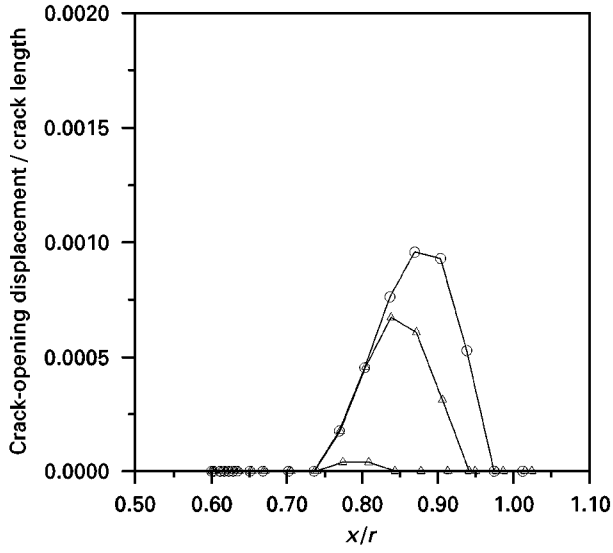

Figure 7 Crack-opening profiles of the circumferential external crack during the early stages of the hydrogen-charging cycle for various normalized charging times. (○), 0.000 575; (△), 0.009 130; (◇), 0.001 410.

overall reduction in the stress values took place and the particle eventually reverted to its stress-free state. This large elevation in the stress values ahead of the crack tip is again associated with the crack-opening behaviour during the discharging cycle. The variation in the crack profiles during the discharging cycle is shown in Fig. 10. At early stages of the discharging, because of rapid diffusion of the hydrogen from the crack faces (Fig. 8), the crack faces open almost immediately, leading to a large increase in the normal stress ahead of the crack tip region. Later, owing to the overall contraction resulting from the loss of hydrogen, crack faces start to close again, as can be seen in Fig. 10.

The evolution of the stress state in a spherical particle having a penny-shaped internal crack during the hydrogen charging cycle is summarized in Fig. 11. In this figure, the crack tip is located at $x/r = 0.4$; x/r values smaller than this value represent the crack wake region and larger values are for the regions ahead of the crack tip. For this case, because of the embedded nature of the crack, the development of the hydrogen concentration profiles were identical with that seen in Fig. 3. As can be seen from Fig. 11, opposite to that seen for the external crack case in the same particle (Fig. 6), large normal stress values develop ahead of the crack tip even at very early stages of the charging. This increase is continuous and reaches a value as high as half the modulus of elasticity. The attainment of this peak value occurred shortly before reaching a fully charged stage; then a slight reduction took place. Nevertheless, the stress level remained significantly high at the fully charged stage.

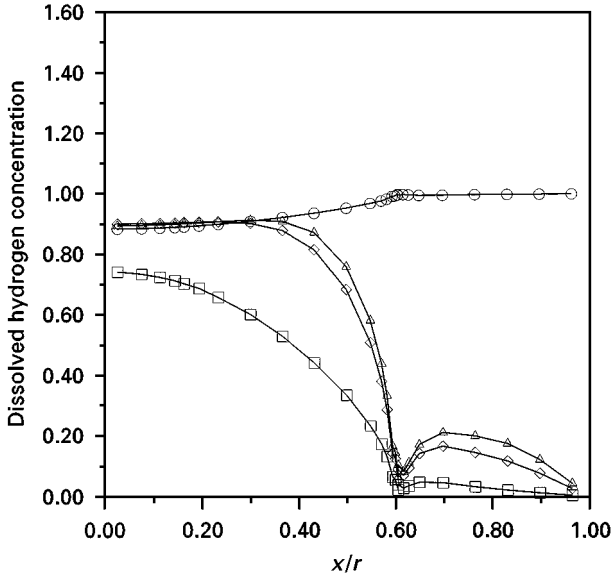

Figure 8 Variation in the hydrogen concentration in the spherical particle with a circumferential external crack during the discharging cycle for various normalized discharging times. (○), 0.020; (△), 0.001; (◇), 0.011; (□), 0.065.

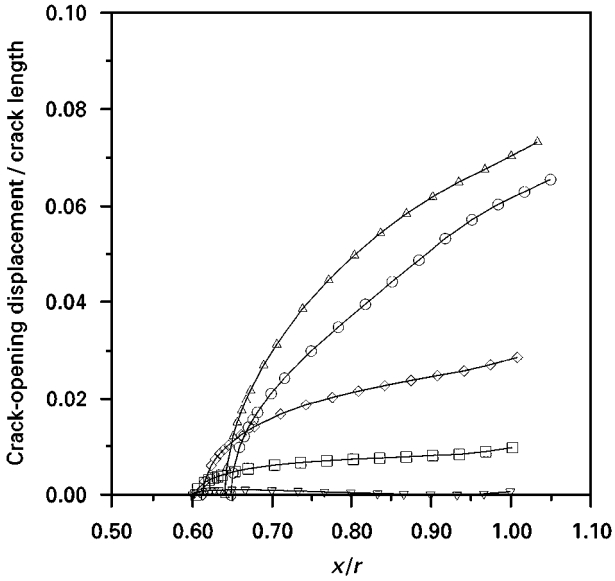

Figure 10 Crack opening profiles of the circumferential external crack during the hydrogen-discharging cycle for various normalized discharging times. (○), 0.001; (△), 0.011; (◇), 0.040; (□), 0.065; (▽), 0.115.

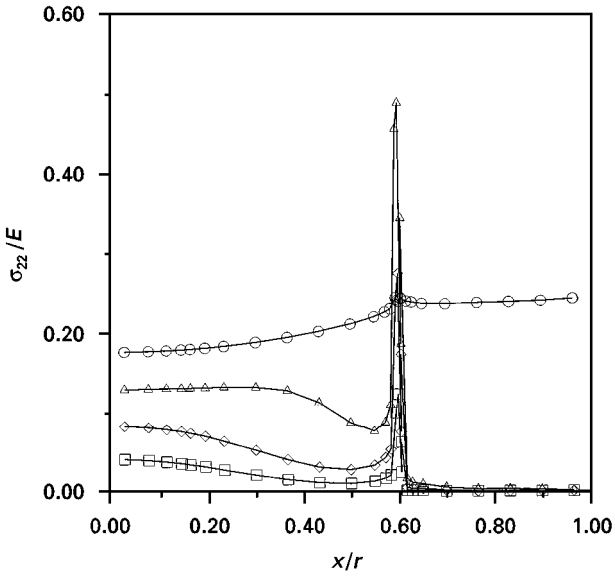

Figure 9 Evolution of the stress state in the spherical particle with circumferential external crack during the hydrogen-discharging cycle for various normalized discharging times. (○), 0.000; (△), 0.001; (◇), 0.011; (□), 0.065.

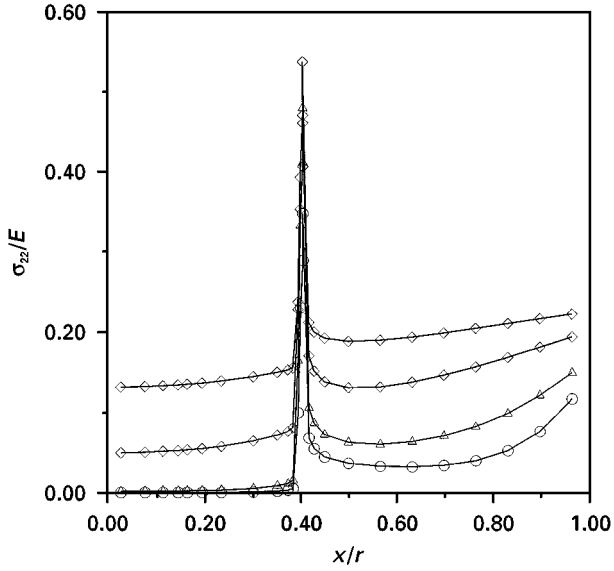

Figure 11 Evolution of the stress state in the spherical particle with a penny-shaped internal crack during the hydrogen-charging cycle for various normalized charging times. (○), 0.0234; (△), 0.0734; (◇), 0.172; (□), 0.272.

The variation in the crack profiles for the time periods given in Fig. 11 are shown in Fig. 12 during the same charging cycle. For this penny-shaped internal crack, the crack faces open up at early stages of the charging cycle and continue to open until swelling of the crack faces occurs as a result of volume expansion as the hydrogen concentration near the crack wake regions reaches higher levels.

Figs 13 and 14 show the stress states and crack-opening profiles, respectively, in the particle containing a penny-shaped crack during the discharging cycle. Again, the zero value of the normalized time corresponds to the fully charged state in the figures. With the loss of hydrogen in regions near the particle surface, stress redistribution takes place and the crack tip stresses relax significantly at very early stages of the discharging cycles. As can be seen from Fig. 13, the stress distribution in the interior regions of the particle becomes quite uniform, as if there is no crack, resulting from the closure of the crack faces due to overall contraction (Fig. 14).

In the next set of simulations the behavior of disc-shaped particles containing a penny-shaped internal crack and a circular surface crack were investigated with the FEM meshes shown in Fig. 15. The volume of this disc-shaped particle and also the size of the penny-shaped crack were identical with that of spherical particles in Fig. 2. Because of the symmetry, only one quarter of the disc was modelled as seen in Fig. 15. The development of the stress states in the disc-shaped

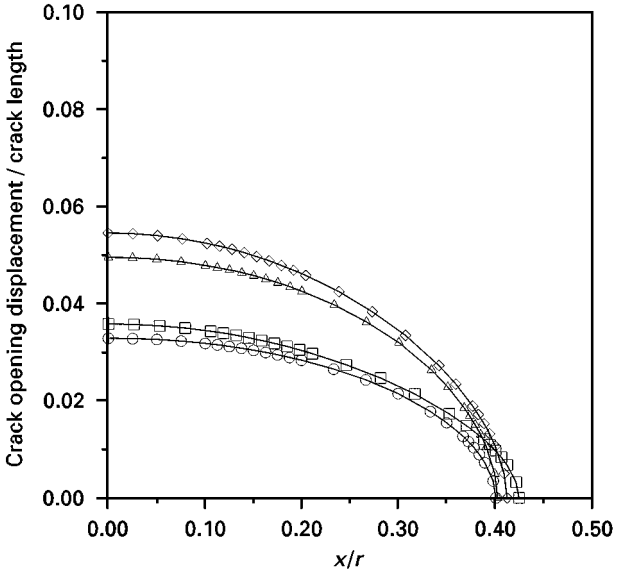

Figure 12 Crack-opening profiles of the penny-shaped internal crack during the hydrogen-charging cycle for various normalized charging times. (○), 0.0234; (△), 0.0734; (◇), 0.172; (□), 0.272.

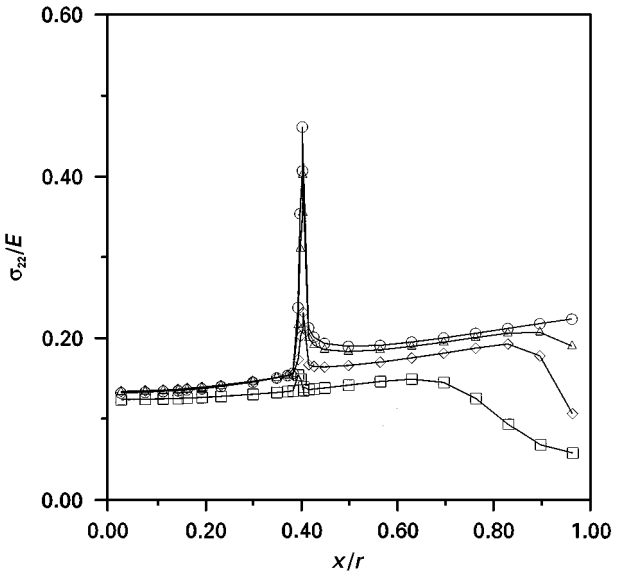

Figure 13 Evolution of the stress state in the spherical particle with a penny-shaped internal crack during the hydrogen-discharging cycle for various normalized discharging times. (○), 0.0; (△), 0.0002; (◇), 0.0005; (□), 0.005.

particle containing the penny-shaped crack during the hydrogen charging cycle is shown in Fig. 16. In this figure, the crack tip corresponds to $x/r = 0.25$; x/r values smaller than this value represent the crack wake region and larger values are again for the regions ahead of the crack tip. The normalized time of 0.0518 corresponds to the fully charged state in the figure. When a comparison is made with the previous spherical particle cases, a significant reduction in the charging time can be observed. This reduction arises from the larger surface-area-to-volume ratio of the disc-shaped particle. As can be seen from Fig. 16, in spite of the presence of an internal crack, the stress distribution in a fully charged state was very uniform which is opposite to that seen for the spherical particle containing a penny-shaped crack (Fig. 11). The shape changes

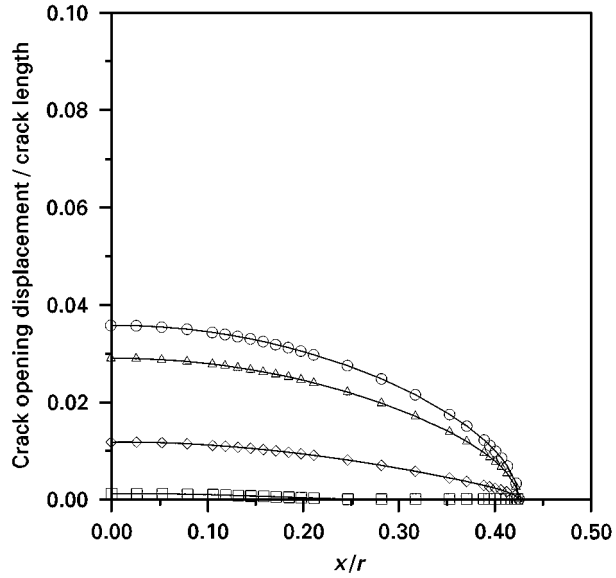

Figure 14 Crack-opening profiles of the penny-shaped internal crack during the hydrogen-discharging cycle for various normalized charging times. (○), 0.0; (△), 0.0002; (◇), 0.005; (□), 0.0050.

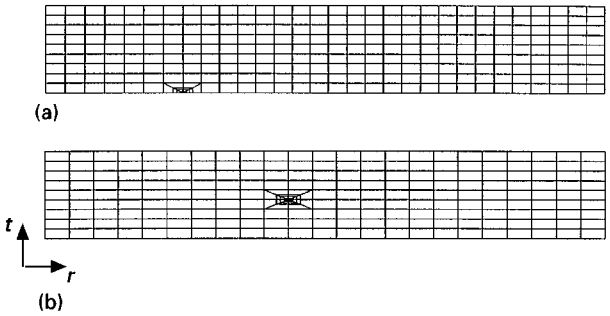

Figure 15 FEM element mesh used during the analyses of disc-shaped particle: (a) for the particle containing a penny-shaped internal crack; (b) for the particle containing a circular surface crack.

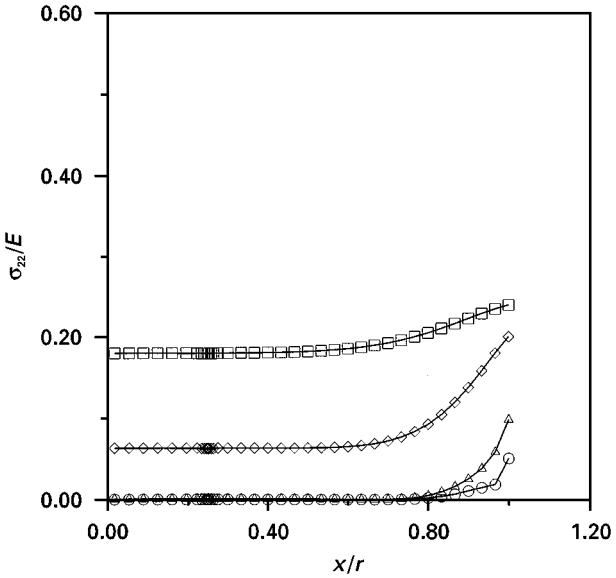

Figure 16 Evolution of the stress state in the disc-shaped particle with a penny-shaped internal crack during the hydrogen-charging cycle for various normalized charging times. (○), 0.001; (△), 0.005; (◇), 0.0254; (□), 0.0518.

of this disc-shaped particle during the same time intervals given in Fig. 16 are shown in Fig. 17. As can be seen from the figure, resulting from the fast diffusion of the hydrogen from both top and side surfaces, a large expansion occurs near the corner regions. This expansion introduces a compression in the central regions, leading to the stress distribution seen in Fig. 16. This can also be substantiated from the crack-opening behaviour during the charging cycle as seen in Fig. 18. The crack opens at very early stages of the charging cycle; however, the amount of this opening is almost three orders of magnitude smaller than that seen for the internal crack in the spherical particle as shown in Fig. 14. Shortly after this opening, the crack tip region closes again owing to the evolution of the compression in the central regions of the particle as described earlier. The variations in the stress values during the discharging cycle of the same particle with the internal crack are summarized in Fig. 19. As can be seen from the figure, no stress elevation takes place during the discharging cycle associated with the aforementioned shape changes.

Figs 20 and 21 summarize the development of the stress states in the disc-shaped particles containing a circular surface crack during the hydrogen charging and discharging cycles, respectively. In these figures, the crack tip is located at $y/t = 0.48$, where t is the half-thickness of the particle; larger values indicate the regions ahead of the crack tip. In the case of a circular surface crack, a stress elevation ahead of the crack tip takes place at very early stages of the charging. As the charging progresses, these high stress values are

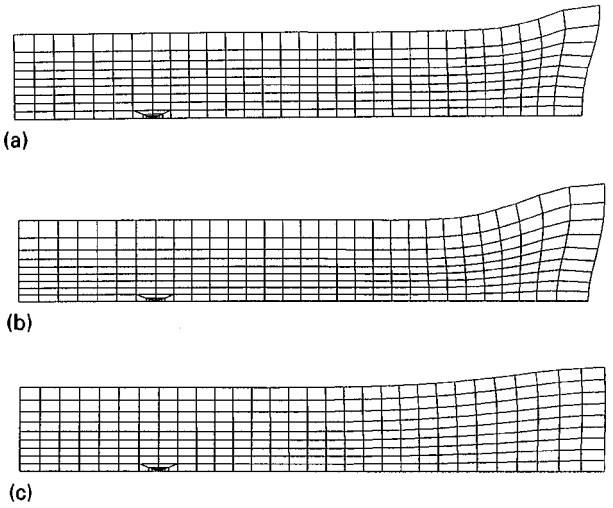

Figure 17 The shape changes in the disc-shaped particle with a penny-shaped internal crack during the hydrogen-charging cycle for normalized times of (a) 0.001, (b) 0.0284 and (c) 0.0518.

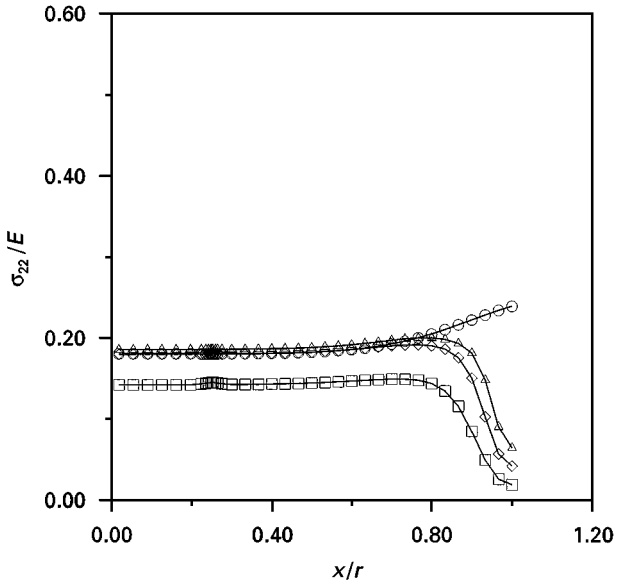

Figure 19 Evolution of the stress state in the disc-shaped particle with a penny-shaped internal crack during the hydrogen-discharging cycle for various normalized discharging times. (○), 0.0; (△), 0.001; (◇), 0.002; (□), 0.005.

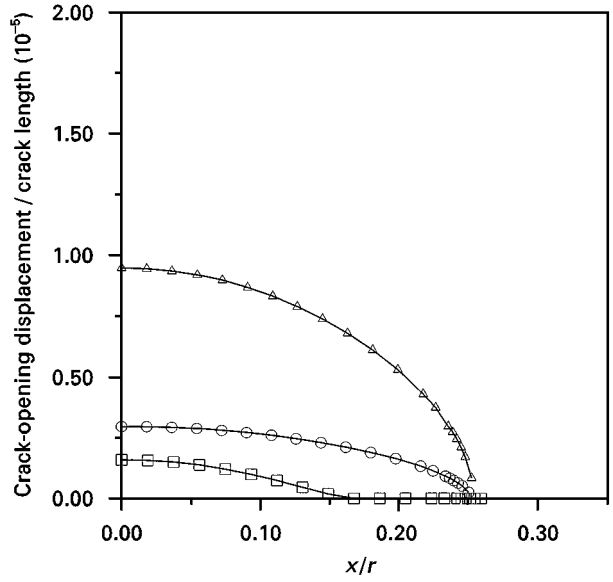

Figure 18 Crack-opening profiles of the penny-shaped internal crack in the disc-shaped particle during the hydrogen-discharging cycle for various normalized discharging times. (○), 0.001; (△), 0.005; (□), 0.0284.

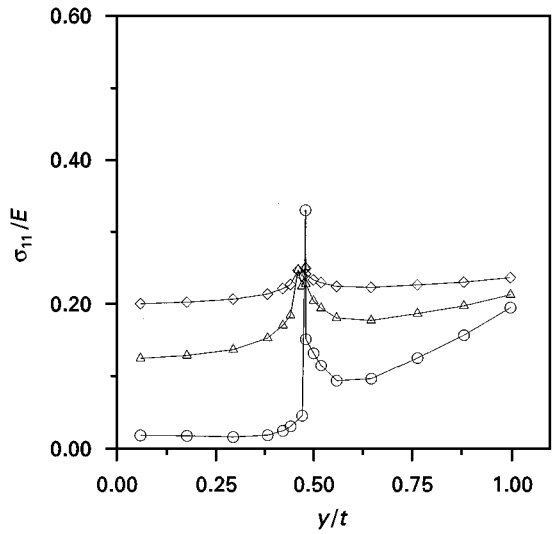

Figure 20 Evolution of the stress state in the disc-shaped particle with a circular surface crack during the hydrogen-charging cycle for various normalized charging times. (○), 0.0050; (△), 0.0234; (◇), 0.0534.

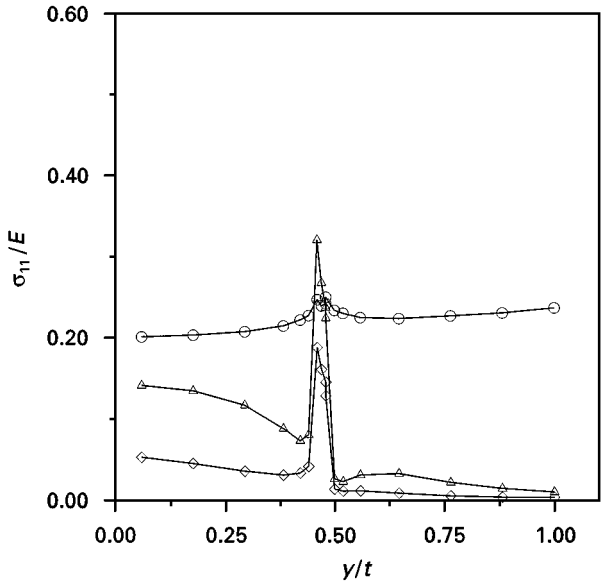

Figure 21 Evolution of the stress state in the disc-shaped particle with a circular surface crack during the hydrogen-discharging cycle for various normalized discharging times. (○), 0.0; (△), 0.001; (◇), 0.005.

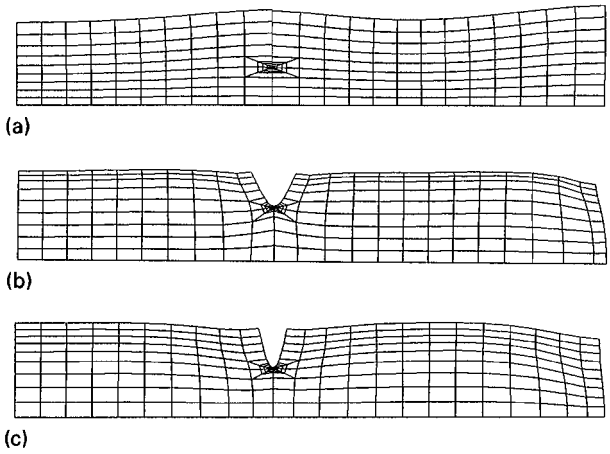

Figure 22 The shape changes in the disc-shaped particle with a circular surface crack during the hydrogen-discharging cycle for normalized times of (a) 0.00 (fully charged stage), (b) 0.001 and (c) 0.005.

redistributed, leading to a uniform distribution of the stress throughout the particle as can be seen in Fig. 20. Similarly, during the discharging cycle, the stress increases again very near the tip region for a very short period of time and then decreases as further discharging takes place (Fig. 21). However, the stress values still remain relatively higher than those occurring in other regions of the particle. When a comparison is made, it will be seen that the maximum stress levels attained ahead of the circular crack in the disc-shaped particle are relatively lower than those seen for both crack cases in the spherical particle (Figs 9 and 11). This behaviour is again associated with the shape changes taking place in the disc-shaped particles during the charging and discharging cycles as shown in Fig. 22. As can be seen from the figure, at the fully charged stage (normalized time equal to zero), the crack was completely closed as a result of swelling of the crack faces and evolution of compressed regions near the crack tip. As discharging continued, an initial opening followed by the closure of the crack faces can be discerned from the figure.

4. Discussion

From the results it appears that large tensile stresses, of the order of 20–30% of the modulus of elasticity, develop in $RENi_5$ particles even in the absence of both internal and external crack-like defects during hydrogenation (Fig. 4). In the case of spherical particles, these stress levels were elevated further to almost half the modulus value in the presence of cracks (Figs 9 and 11). However, for identical crack lengths in a spherical particle, while this elevation takes place almost throughout the whole charging cycle for penny-shaped internal cracks (Fig. 11), it only occurs for a very short period of time during the discharging cycle for the circumferential external cracks (Fig. 9). Since the crack driving force is only available for a short period of time, for initial cracks of identical sizes, the survival time for the external cracks will be much longer than for the internal cracks.

Apart from the faster charging–discharging cycles, owing to the larger surface-area-to-volume ratio, it appears that the disc-shaped particles with initial cracks also offer better resistance to fracture than the spherical particles do. As can be seen in Figs 16 and 19, there was no stress elevation ahead of the penny-shaped internal cracks in disc-shaped particles during both charging and discharging cycles. The stress increases seen ahead of the circular surface cracks (Figs 20 and 21) were again smaller than those seen for both external and internal cracks in the spherical particles (Figs 9 and 11) and these elevations also occurred for very short time periods.

During the analysis, it was assumed that both the diffusion parameters and the modulus of elasticity remained constant during hydrogenation cycles; in spite of these simplifications, however, the present results clearly demonstrate the role of crack morphology and particle shape in the fracture behaviour of $RENi_5$ powders.

5. Conclusions

In this study, the development of the stress states in $RENi_5$ particles during hydrogen charging and discharging cycles was investigated using coupled diffusion–deformation FEM analyses. The results indicate the following.

1. Large tensile stresses, of the order of 20–30% of the modulus of elasticity, develop in the particles even in the absence of both internal and external crack-like defects.

2. The internal and external cracks behave differently from each other during hydrogen charging and discharging cycles. Therefore, the fracture resistance of particles containing external cracks will be different from that of the particles having internal cracks.

3. The disc-shaped particles, in addition to having faster charging–discharging cycles, may offer better resistance to fracture than the spherical particles do.

Acknowledgements

This work was performed for the US Department of Energy by Iowa State University under Contract W-7405-82. This research was supported by the Director of Energy Research, Office of Basic Sciences. The author wishes to thank to Dr T. Ellis and Dr O. Buck for bringing the problem to the attention of the author.

References

1. J. H. N. VANVUCHT, F. A. KUIJPERS and H. C. A. M. BRUING, *Philips Res. Rep.* **25** (1970) 133.
2. M. H. MINTZ and Y. ZEIRI, *J. Alloys Compounds* **216** (1994) 159.
3. K. H. J. BUSCHOW and H. H. VANMAL, *J. Less-Common Metals* **29** (1972) 203.
4. Z. ZUCHNER and T. RAUF, *J. Less-Common Metals* **172–174** (1991) 611.
5. R. WANG, *Mater. Res. Bull.* **11** (1976) 281.
6. R. S. BARSOUM, *Int. J. Numer. Meth Engng* **10** (1976) 25.
7. S. B. BINER, O. BUCK and W. A. SPITZIG, *Engng Fracture Mech.* **47** (1994) 1.

Received 7 May 1997
and accepted 2 April 1998